Exploring the response of a resistive soot sensor to AC electric excitation

Middelburg, L.M.; Ghaderi, M.; Visser, J.H.; Wolfenbuttel, R.F.

DOI
10.1016/j.jaerosci.2020.105568

Publication date
2020

Document Version
Final published version

Published in
Journal of Aerosol Science

Journal of Aerosol Science 146 (2020) 105568

Contents lists available at ScienceDirect

Journal of Aerosol Science

journal homepage: http://www.elsevier.com/locate/jaerosci

Exploring the response of a resistive soot sensor to AC electric excitation

L.M. Middelburg [a,*], M. Ghaderi [b], D. Bilby [c], J.H. Visser [c], R.F. Wolffenbuttel [a,b]

[a] Department of Microelectronics, Faculty of EEMCS, Delft University of Technology, Mekelweg 4, 2628CD, Delft, the Netherlands
[b] Chalmers University of Technology, Department of Microtechnology and Nanoscience, EMSL, Kemivägen 9, 412 58, Gothenburg, Sweden
[c] Research and Advanced Engineering, Ford Motor Company, Dearborn, MI, 48121, USA

ARTICLE INFO

Keywords:
Particulate matter sensing
Impedance spectroscopy
Dendrite growth
Electrostatic soot sensor
Aerosol emissions
Electrophoresis
Exhaust gas aftertreatment
On-board diagnostics

ABSTRACT

The resistive particulate matter sensor is a simple device that transduces the presence of soot through impedance change across inter-digital electrodes (IDEs). We investigate the information provided by impedance spectroscopy over the frequency range from 100 Hz to 10 kHz for two purposes. The first is to investigate the opportunities for an improved sensor response to particulate matter (PM), based on the additional information provided by the measurement of both the in-phase (resistive) and out-of-phase (capacitive) components of the change in impedance over this frequency range as compared to DC resistance measurement only. Secondly, the origin of the capacitive response of the device is investigated from the perspective that soot on the device is in the form of bendable dendrites that grow in three dimensions. An IDE structure with the housing acting as an additional suspended electrode for introducing a controllable vertical electric field component has been used for this purpose. The formation of dipoles, due to bending of the charged dendrites, is found to be the source of the capacitive response. Simulation of electrostatic soot deposition reinforces dendritic self-assembly mechanisms, driven by charged particle trajectories along electric field lines. Optical microscopy confirms that dendrites growing out of the substrate plane are sensitive to electric and flow forces, bending when force balances are appropriate. We also apply impedance spectroscopy under varying electric field strengths, showing that capacitive response is only observed when conditions are conducive to dendrite bending in response to the applied AC electric fields.

1. Introduction

The adverse effect of automotive emissions on health and the environment has resulted in tight regulations on maximum emission of unburned hydrocarbons, nitrogen-oxides (NO_x) and particulate matter. In addition, concerns on global warming and use of natural resources has resulted in targets on fuel efficiency and consequently on CO_2 emission. Exposure to particulate matter (PM) leads to increased risk of mortality due to cardiorespiratory disease (Newell, Kartsonaki, Lam, & Kurmi, 2017). In order to limit release of PM from combustion engines used in transportation, exhaust aftertreatment includes a diesel particulate filter (DPF). PM sensors, installed downstream of a DPF, verify filter health in situ; when a filter fails, early detection and replacement minimizes PM release over the lifetime of a vehicle.

* Corresponding author.
E-mail address: l.m.middelburg@tudelft.nl (L.M. Middelburg).

https://doi.org/10.1016/j.jaerosci.2020.105568
Received 24 September 2019; Received in revised form 22 February 2020; Accepted 8 April 2020
Available online 19 April 2020

Practical on-board diagnostic (OBD) PM sensors must not only be sensitive and selective to soot, but they must also be inexpensive and survive harsh exhaust conditions. These competing requirements result in a variety of possible solutions; many transduction mechanisms have been considered for OBD PM sensors including high-voltage electrostatic (Warey, Hendrix, Hall, & Nevius, 2004), (Bilby, Kubinski, & Maricq, 2016), diffusion charging (Rostedt et al., 2017), and optical (Zhang, del Re, & Fuerhapter, 2017) techniques. However, the most prolific OBD PM sensors are based on simple resistance or capacitance measurements of deposited soot (Bartscherer & Moos, 2013; Binnig, Fuchs, Collantes, & Volpp, 2017; Feulner et al., 2015; Fragkiadoulakis, Geivanidis, & Samaras, 2018; Grondin et al., 2016, 2019; Hagen et al., 2015, 2018).

Resistive PM sensors, also referred to as conductometric soot sensors, encompass a category of devices composed of inter-digitated electrodes (IDE) supported on ceramic substrates. Upon exposure to a soot containing gas flowing over the sensor surface, soot particles are deposited and a conducting path is formed between the IDE. As soot accumulates on the IDE, the sensor develops an idiosyncratic response; there is a long period of time where the device displays no signal because soot has not yet bridged the IDE. It is notable that this behavior creates ambiguity about the presence of soot aerosol. The amount of time that it takes generating the signal is inversely proportional to the cumulative amount of soot on the IDE. Thus, lower soot concentrations require longer delay times for generation of a signal and confirmation of a DPF leak. Following verification of DPF health, subsequent measurements may be performed after burning off accumulated soot via an integrated heater.

It is desirable to decrease the amount of time required for diagnosing a leaky DPF at a given soot concentration in order to increase the frequency of DPF characterizations and to decrease exposure to damaging contaminants (Binnig et al., 2017) while electrical potential is active on the IDE. Acceleration of the response time of resistive PM sensors has been investigated through optimization of applied bias (Grondin et al., 2016). Increased bias leads to increased electrostatic soot capture and therefore faster response. Unfortunately, increased bias also leads to Joule heating of the deposited soot bridges (Hagen et al., 2018). As the deposited soot undergoes self-heating it creates a thermophoretic force that reduces deposition (and causes self-destruction), leading to a limitation in sensitivity enhancement with increased bias (Grondin et al., 2019). Response time reductions have also been investigated through application of small device modifications and alternative measurement modes such as capacitance (Hagen et al., 2015) and parallel resistance (Bartscherer & Moos, 2013). Despite these efforts, the presence of the typical delay in the shape of the signal in resistive soot sensors is inevitably caused by the way of operation.

The first aspect of this work is to explore the potential of impedance spectroscopy for measuring the full IDE impedance over a frequency range between 100 Hz and 10 kHz in an attempt to achieve improved sensitivity, a reduced response time or additional information on the PM size distribution. The results to be presented indicate that the gains achieved by full impedance measurement are limited, which implies that the intrinsic soot deposition mechanisms active within the resistive PM sensor are strongly intertwined with design changes and signal interpretation. Therefore, an improved understanding of all of the interacting physics is required in order to build a faster sensor. This second aspect of this work is the investigation of the influence of electric fields on the capacitive

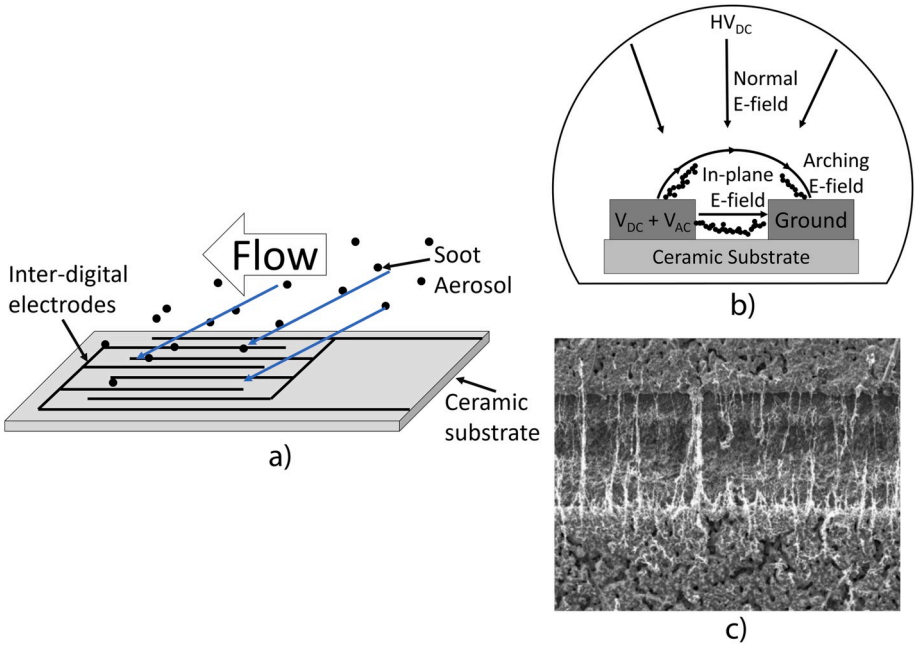

Fig. 1. a) Schematic diagram of resistive PM sensor construction; the inter-digitated electrodes are supported by a ceramic substrate. The electrodes are held at different electrical potential, and the electric field between the electrodes and metal housing enables electrophoretic soot capture. b) Schematic diagram of electric field orientation around an IDE pair including in-plane and normal components. Soot particles move along field lines and are captured on the electrodes. The particles assemble into dendrites which also follow field lines. c) SEM image showing soot dendrites bridging the gap between inter-digitated electrodes.

response of a resistive PM sensor.

We propose a phenomenological explanation for the capacitive response of a resistive PM sensor that relies upon the growth and motion of soot dendrites on the sensor IDE. We support the model with simulation, optical microscopy and impedance spectroscopy of soot dendrites in the presence of orthogonal electric fields. Our findings contribute to the understanding of subtleties of soot dendrite physics on PM sensor response by showing that the three-dimensional nature of soot dendrite growth and the freedom of dendrite motion are important considerations in resistive PM sensor signal generation and interpretation. The organization of the paper is as follows. After the presentation of the operation of the IDE structure, the modeling as a circuit comprising a parallel resistor-capacitor configuration is described, which would enable the interpretation of the impedance measurements, as part of objective 1. Section 3 continues with Finite Element Modeling (FEM) of electrophoresis. These results are needed for enabling an analysis of electric field-dependence of dendrite growth within the framework of objective 2. These models are experimentally validated in Section 4 and interpreted in Sections 5 and 6.

2. *Operation of the resistive soot sensor*

The resistive soot sensor is a deceptively simple device, as shown schematically in Fig. 1. Electric potential is applied across the IDE and between the IDE and metal housing surrounding the sensor. Soot is natively charged through combustion (Maricq, 2008) and is carried by flow through the sensor and along the IDE. Soot capture occurs as competition between electrophoretic forces and aerodynamic drag forces move particles along E-field lines and parallel to the substrate, respectively. When soot arrives on the substrate, it is observed to self-assemble into dendrites due to the forces acting on the aerosol.

Particles travelling through practical PM sensor devices experience thermophoresis, flow driven impaction, Brownian motion and electrophoretic forces. The design of the device and operating environment ultimately dictate the relative importance of each of these forces in sensor operation. In some cases, thermal gradient and electric field driven particle motion are the primary sources of deposition; the forces that drive particle coagulation, such as diffusion, are of secondary importance in PM sensor soot capture (Fragkiadoulakis et al., 2018). Dendritic soot morphologies, rather than uniform coatings, are observed to form when conductive materials are captured in electrostatic precipitator devices (Riehle & Wadenpohl, 1996). Because of this, high-voltage (Bilby et al., 2016) and conductometric (Grondin et al., 2016) PM sensors also exhibit soot dendrite growth. This dendrite morphology forms due to enhanced attraction of subsequent particles to the localized electrical perturbation from prior aggregate depositions, as shown in simulations of particle deposition under shearing flow (Teike, Dietzel, Michaelis, Schomburg, & Sommerfeld, 2012). Additionally, the character of the dendrites which form is sensitive to soot properties (Grob, Schmid, Ivleva, & Niessner, 2012), electric potential (Grondin et al., 2019), and other acting forces (Maricq & Bilby, 2018).

3. Modeling

In the simplest description, the resistive PM sensor is a capacitor that develops a current leak as soot dendrites bridge the inter-electrode gap. The amount of time that it takes for a current leak to appear can be modeled as the amount of time that it takes for a soot dendrite to grow across the gap. Then, as more bridges create inter-electrode contact their contribution adds in parallel. Quantized, kinetic descriptions of dendrite growth, such as those in Bilby et al. (2016) and Grondin et al. (2019) predict the delay and current rise behavior of resistive PM sensors quite well. Such a model could be applied to predict the rate of capacitor electrode surface area change as a function of dendrite growth. However, this type of model does not accommodate the influence of dendrite freedom-of-motion. In order to include this characteristic, we propose an alternate model that more closely matches experimental observations of capacitance behavior that we will discuss in later sections.

We describe the PM sensor as a capacitor and build our model from the perspective of the relative dielectric permittivity. The electrical polarization, P, is related to the spatial density of dipoles of an average charge, q, separated by an average distance, x.

$$P = \frac{dp}{dV} = \frac{dq \cdot x}{dV} \tag{1}$$

We propose that the dipoles which affect resistive PM sensor capacitance are formed due to physical bending of soot dendrites. The dendrites carry charge due to being in contact with electrically biased electrodes, and they are perturbed from an equilibrium position by AC or changing bias. This model relies upon the ability of dendrites to move in response to bias; physically constrained dendrites would not contribute to displacement-derived capacitance. Thus, the effective dipole charge per volume is related to the spatial number density of dendrites, N, and effective charge per dendrite, q_{avg}.

$$dq = N \cdot dV \cdot q_{avg} \tag{2}$$

Then, when the AC electric field, E, is applied, the dendrites move a distance, x, in response to this force. The distance that the dendrite is displaced is proportional to the freedom of motion of dendrites as described by an effective stiffness, K_{eff}.

$$F_E = qE = K_{eff}x \tag{3}$$

We can then rewrite the electrical polarization in terms that depend on soot dendrites, and use this to describe the relative dielectric constant, ε_r, as polarization is a component of the electric displacement, D.

$$D = \varepsilon_0 E + P = \varepsilon_r \varepsilon_0 E \tag{4}$$

$$\varepsilon_r = 1 + \frac{N q_{avg}^2}{\varepsilon_0 K_{eff}} \tag{5}$$

Since capacitance is proportional to relative dielectric constant, this model makes it clear that charged soot dendrite motion can contribute to capacitive PM sensor response. In this description, dendrites without sufficient freedom of motion do not contribute to capacitive response. A linearized parallel resistance can be used for interpretation of the impedance spectroscopy data. However, more elaborate modeling is needed for interpretation of the physics of soot deposition. Although the modeling in terms of a capacitor in parallel to a linearized leak resistor is shown to be adequate for the interpretation of the impedance measurements in the next section, it is insufficient for gaining understanding on how the interplay between flow and electric field affects electrophoretic deposition of soot and dendrite growth. Therefore, we perform 2D finite element simulations (COMSOL Multiphysics v. 5.4) of particle deposition in an 800 μm tall flow channel.

The flow field is calculated with a finite element method, yielding laminar flow with a maximum of 2 mm s^{-1} at the center of the channel. The static electric field is also calculated for a set of five electrodes of about 45 μm width and gap, alternating 0 V and 40 V potential (the top of the flow channel is also at 0 V). As shown in Fig. 2, the normal component of the electric potential above positive and grounded electrodes is different. Above a positive electrode, negatively charged particles are attracted and positively charged particles are repelled. Field strength decays with increased distance above the electrode, so interaction between particle mobility and flow sweep-out will create a critical capture height, above which no particles are captured. Above a grounded electrode the gradient in potential takes on a different shape; positive particles above a critical distance are repelled from the ground electrode due to the far-reaching field between the top of the flow channel and the positive electrode. This results in an electrically defined critical capture distance for positive particles, as well as a height where negative particles should concentrate.

Particle deposition is simulated by tracking the motion of 80 nm spherical particles of +1, 0 and −1 charges in the static flow and electric fields which were calculated earlier. Brownian motion is considered to be negligible in our room temperature experiments. Thermophoretic forces are considered as position-independent force and superimposed on the electric field. Therefore these are not considered here. The simulated particles are 80 nm, which is the average particle size in a typical exhaust gas soot (Harris & Maricq, 2001). The variations in size only result in a different mobility and do not change the overarching trends in particle capture. The charged particles get strongly attracted toward opposing IDE electrodes. Because flow is orthogonal to the IDE pattern, we observe arching particle trajectories, as shown in Fig. 2.

Particles entering below the critical capture height, are typically captured at the electrodes and near the inter-electrode gap. Additionally, more particles are captured on the positive electrode due to the interaction of flow and electric field. As the electrophoretic force is weaker, only the slow moving neutral particles near the surface are get affected by the electric field. These particles are also more likely to deposit at the corners of the IDE where gradient of the electric is strongest. This arching trajectory creates concentration of deposition, a first step that is expected to help enhance dendrite growth rate.

Particle trajectory simulation under static electric fields ignores the influence of particle-particle interactions, especially missing the influence of pre-deposited particles on subsequent deposition. We expect the influence of deposited particles to be critical for dendrite growth. Therefore, we re-calculate the static electric field with geometric features that mimic pre-deposited, dendrite-seed particles. The seed particles are modeled at various lengths and are placed near the downstream side of an electrode. Each seed is

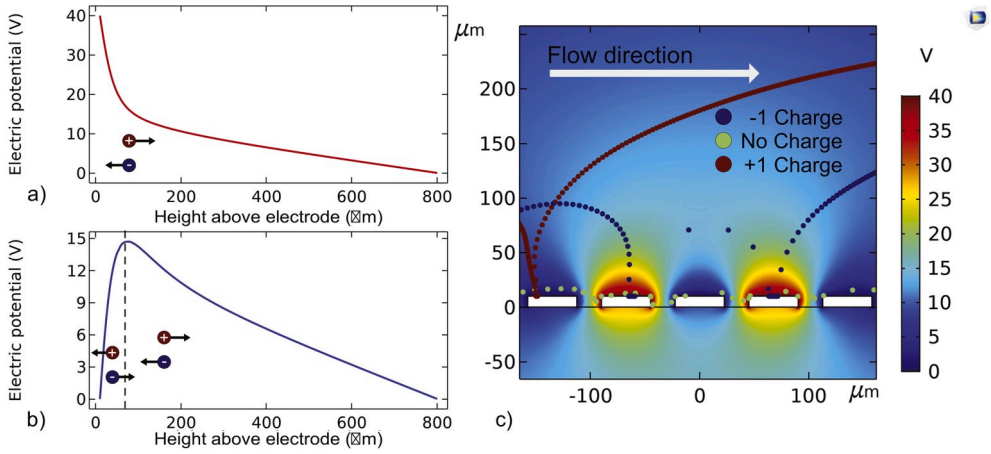

Fig. 2. a) Normal component of electric potential profile over the center of a positive electrode. The field strength decays with increasing distance from the electrode, but the sign remains constant. This results in attraction of negative particles and repulsion of positive particles. b) Normal component of electric potential profile over the center of a grounded electrode. The potential increases up to about 100 μm, then decays. This results in two regimes: near the electrode positive particles are attracted and negative particles are repelled; far from the electrode positive particles are repelled and negative particles are attracted. This results in an electrically defined critical capture height. Above this height, no positive particles are captured. c) simulated particle trajectories in static electric and flow fields for 80 nm, spherical, singly charged and neutral particles. Interplay between flow and electrically driven particle mobility results in arching flow trajectories with capture of charged particles at the electrodes.

arbitrarily designed to be a square with 1000 nm side length, with a quarter of its size overlapping with the electrode (for the initial seed) or the previously deposited seed, thus each seed effectively resembles a 500 nm growth of the simulated dendrite in the diagonal direction. This growth is equivalent to the deposition of about 9–10 average soot particle on the tip of the dendrite. The seed is also given the same electric potential as the electrode. As shown in Fig. 3, the seed dendrite creates a concentration of electric field lines that leads to increasingly localized particle capture at repeated simulations. After each seed growth step, the soot is deposited at the tip of the dendrite seed, which is indicative of growth of long dendrite structures between the electrodes. At the same time, the inclusion of the dendrite seed does not dramatically affect the total number of particles captured on positively biased and grounded electrodes. This result is consistent with electrostatically driven, preferential self-assembly of deposited soot into dendritic structures.

Our simulation also shows that the interaction between electric and flow fields is critical for where on the IDE structure a dendrite will initiate, how fast particles are delivered per IDE area, as well as critical in determining ultimate particle capture height. These factors are important because concentrated deposition of a larger sampled flow volume leads to faster growth of dendrites, which in turn is expected to lead to faster resistive signal generation. One key point that our particle deposition simulation has neglected is the impact of the shape and magnitude of electric and flow field strength on dendrite orientation. This is a complicated topic, tied to the development of dendrite morphology, so we investigate this experimentally.

4. Experimental

The influence of electric field strength and orientation on the resistive PM sensor is investigated through optical microscopy and impedance spectroscopy. Soot aerosol is generated with a Jing miniCAST 5201c which burns propane in a diffusion flame to reproducibly create a particle size distribution with a mean geometrical mobility diameter near 80 nm. The aerosol is subsequently diluted with nitrogen in a Dekati FPS 4000 dilutor before being drawn by downstream pumps through the PM sensor flow housing. Soot concentration is monitored by a DustTrak II model 8530 and is on the order of 0.51 mg m^{-3} in most tests.

The PM sensor used for in-situ optical microscopy observation of dendrite behavior is a 3D printed flow housing that holds two, 8 mm wide substrates orthogonal to cover slide glass. The glass windows enable in-situ microscopy of out-of-plane dendrite growth. One substrate includes the IDE, whereas the other is a planar, steel electrode. This orientation allows for direct application of out-of-plane bias, similar to that afforded by the housing that surrounds conventional resistive PM sensors. The IDE transducer was prepared by painting silver ink followed by laser structuring and sintering. The IDE pattern includes 8 electrodes of 475 μm width separated by 110 μm gaps. The flow channel between the planar electrode and IDE is 730 μm tall. The IDE pattern is perpendicular to flow and flow is parallel to the substrates at a rate of 0.5 L min^{-1} at room temperature.

The PM sensor used for impedance analysis is constructed from components of a commercially available automotive PM sensor. It is constrained in a metal flow housing that forces aerosol-laden flow to pass through the sensor and across the IDE. Both resistive PM sensors used in this study allow for application of in-plane and normal electric field components by adjusting the IDE and metal housing electrical potentials.

Impedance analysis is performed with a Solartron 1260 analyzer, and concurrent electrical biasing of the metal flow housing is applied with a Stanford Research Systems PS365 HV power supply. DC bias measurements during optical microscopy are performed

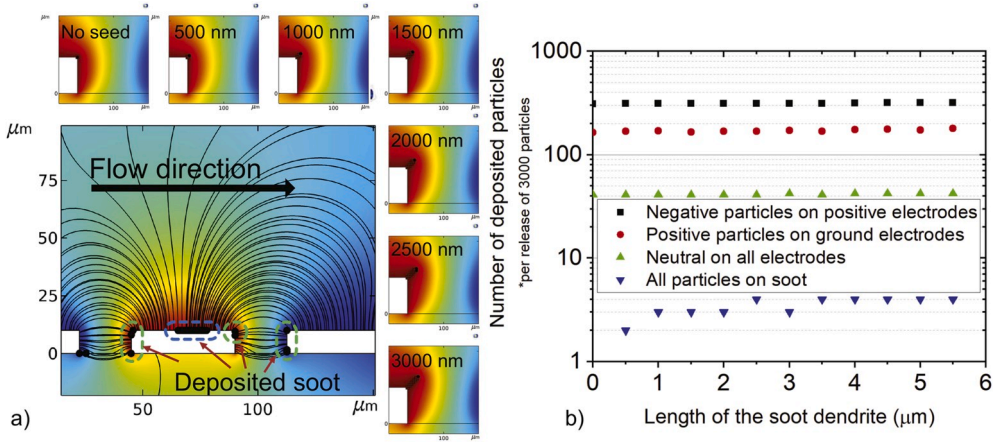

Fig. 3. a) Calculated static electrical potential map for IDE structure with a seed dendrite on the downstream side of the positive electrode in the middle. The electric field lines highlight the enhanced capture propensity of the seed dendrite. The charged particles get deposited over the surface of the electrodes, and the neutral particles over the corners resulting in dendrite growth. The inserts show growth of a dendrite 'seed' at an area where most particles gets deposited. Note 1: the size of soot particles (black spots) are plotted 5x bigger than the actual diameter for better visibility. Note 2: In all cases ploted here, there are up to 3 particles deposited overlapping. b) The number of captured particles on various features of the geometry is plotted as a function of length of the seed dendrite. The seed dendrite does not dramatically affect the total number of particles captured on positive and negative electrodes. The total number of particles captured on the positive electrode is larger than those captured on the negative. As the length of the seed dendrite increases it captures more particles. This leads to self-propagating assembly into a dendrite.

with a Keithley 2420 source-measure unit in addition to the aforementioned HV power supply. The raw impedance data (magnitude and phase) is mapped on the equivalent model parameters, c.q. parallel capacitance and resistance. A schematic overview of the measurement setup is included in Fig. 4.

5. Results

In order to learn about the influence of electric field orientation and strength on dendrite freedom of motion, we perform optical microscopy. This experiment yields qualitative information about how dendrites grow out of the IDE plane, as well as information about dendrite response to applied forces. Three variations in relative electric field strength are investigated, all with constant flow shear; 1) large in-plane E-field: 98 V between the IDEs and 0 V out of plane; 2) large in-plane E-field with normal E-field: 98 V between the IDEs and 147 V out of plane; 3) small in-plane E-field with normal E-field: 7V between the IDEs and 147 V out of plane. These conditions lead to different relative contributors to electric forces which pull on the charged soot dendrites. As shown in Fig. 5, soot dendrites of 10 μm–50 μm are observed to grow out-of-plane, and the different electric forces result in subtle differences in dendrite orientation.

A large in-plane bias leads to soot dendrite growth both in and out of the IDE plane. Microscopy reveals the out-of-plane dendrites, while simultaneous resistance measurement shows that in-plane, inter-electrode bridges have formed. The out-of-plane dendrites stand due to the arch-shaped fringing component of the in-plane field; in-plane application of electric bias leads to a normal E-field component that compels soot dendrites to grow upward. Interestingly, there are occasional out-of-plane dendrites growing outward from in-plane dendrites in the inter-electrode gap. In addition to being strong enough to hold the dendrites in a standing position, the normal E-field is strong enough to hold dendrites to bending angles inclined against flow shear. This is clearest in dendrites which are very near the inter-electrode gap, where bending angles follow the arching E-field lines. When the in-plane bias is removed, the dendrites are observed to fall and lay in the plane of the substrate. This is evidence that the dendrites were not mechanically stable without the influence of electric forces.

A large in-plane bias combined with an added out-of-plane bias leads to similar observation of in-plane and out-of-plane soot dendrite growth. In this case, the E-field near the inter-electrode gap is still dominated by the in-plane bias. The dendrites are also confined to follow the arching field lines against flow shear forces. When the out-of-plane bias is removed, a small population of soot dendrites which grow on the IDE away from the gap are observed to fall down. This reveals that the out-of-plane bias does influence the dendrites in addition to the in-plane bias. The remaining population of dendrites, including those near the inter-electrode gap, fall only when the in-plane bias is removed.

When a small in-plane bias is combined with an added out-of-plane bias, we once again observe both in-plane and out-of-plane soot dendrite growth. All dendrites show a noticeable bend angle along the flow direction, indicating that the flow shear force is stronger than the normal electric force that dominated in the previous two experimental cases. When the out-of-plane electric bias is removed, all dendrites fall, indicating that the normal field component of low in-plane applied bias is not sufficient to hold dendrites in a standing position.

The optical microscopy results confirm that soot dendrites grow along electric field lines, even out of the IDE plane. Our model for capacitive PM sensor response requires dendrites to be physically moved by electric forces, so direct observation that dendrites are pulled by electric and flow forces is consistent with this view of sensor behavior. Moreover, when the relative magnitude of these forces is adjusted, the dendrites grow in or move to a different equilibrium. In other words, when the dendrites are stabilized by large electrical forces, small perturbations such as flow shear or lesser electric bias adjustments do not result in appreciable motion of soot dendrites.

Next, we perform impedance spectroscopy in order to learn about the influence of applied bias on capacitive response of a resistive PM sensor. We interrogate a set of conditions which affect the relative electric forces that define dendrite freedom of motion in the device. We apply small AC bias, 0.5 V or 3 V, across the IDE while simultaneously applying either a small or large DC bias, 0 V, 5 V or 40 V, across the IDE. At the same time, we apply out-of-plane bias of either 0 V or 500 V. These bias levels produce similar order of magnitude electric fields as in the microscopy experiment due to the different geometry of the PM sensors used.

The magnitude of the (complex) impedance $|Z|$ and the phase shift of the impedance θ plots are included in Fig. 6. The $|Z|$ plot

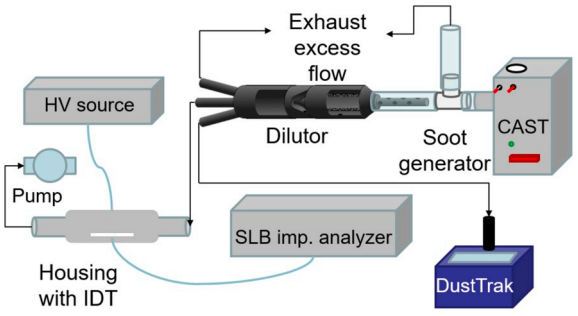

Fig. 4. This setup allows for independent control of aerosol concentration and flow.

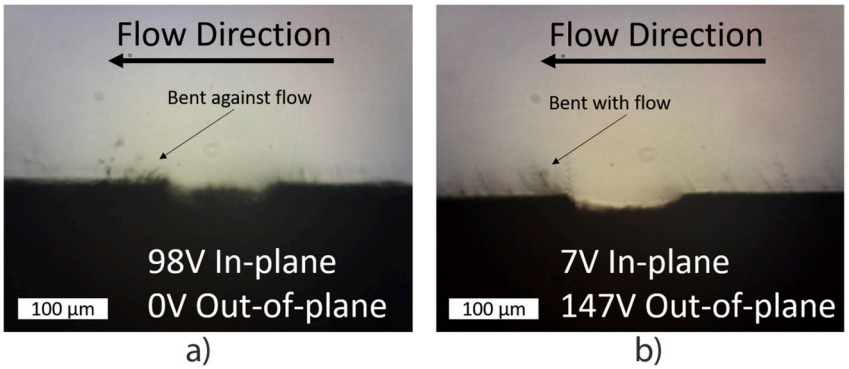

Fig. 5. a) Soot dendrites growing out of the IDE plane in the presence of large bias applied in the plane of the IDE. The dendrites grow on the IDE metal and near the inter-IDE gap. Dendrites which grow in-plane are not easily visible from this perspective. The large in-plane E-field leads to dendrites following field lines despite shearing flow forces; dendrites at the inter-IDE gap on the downstream side of the gap bend against the flow due to electrical forces. b) Soot dendrites growing out of the IDE plane in the presence of small bias applied in the plane of the IDE along with a normal E-field. The dendrites grow on the IDE as well as near the inter-IDE gap. Electrical forces are weaker than flow shear, so dendrites are all observed to bend in the direction of flow.

implies a parallel RC network, where the response starts purely capacitive. When deposition time increases, the pole shifts towards higher frequencies, thus showing-up in the magnitude part of the bode plot. The reduction of the magnitude response at low frequencies reveals the almost exponential reduction of resistance at the onset of dendrite bridging. The measured phase response is almost flat -90° at $t = 0$ min, after which the pole is pushing the phase shift to higher frequencies. The gradual increase of the phase in time at higher frequencies reveals the gradual change in capacitance with soot buildup.

The raw impedance data was mapped on the equivalent circuit model, and the parallel resistance and capacitance at a frequency of 4.8 kHz are plotted over time, as included in Fig. 7. As shown in this Figure, the extracted resistance and capacitance evolve differently over time as a function of applied electrical potentials. We chose to plot the R and C data at a single frequency of 4.8 kHz, because the data beyond this frequency provided better fitting with our equivalent circuit model. At low frequencies parasitic components results in a deviation from the modeling based on a parallel RC circuit.

All of the impedance-derived resistance traces exhibit typical resistive PM sensor response. First, there is a period of time where the resistance does not change because dendrites have only begun to form. Next, there is a period where resistance begins to fall as dendrite bridges sporadically make connection between the IDEs. The amount of time that the sensor spends in the pre-bridge state varies over a range of minutes depending on the applied electrical biases. The in-plane bias plays an important role directing dendrite orientation orthogonal to the IDE fingers; strong in-plane bias causes dendrites to more readily connect the two leads of the IDE. The out-of-plane bias helps bring more particles in for capture, too. Thus, the fastest drop in resistance occurs for high in-plane and high out-of-plane bias. Moderate delays before resistance drop occur when large in-plane bias is paired with no out-of-plane bias or when moderate in-plane bias is paired with out-of-plane bias. The slowest resistance decrease response occurs for low in-plane bias. These behaviors are

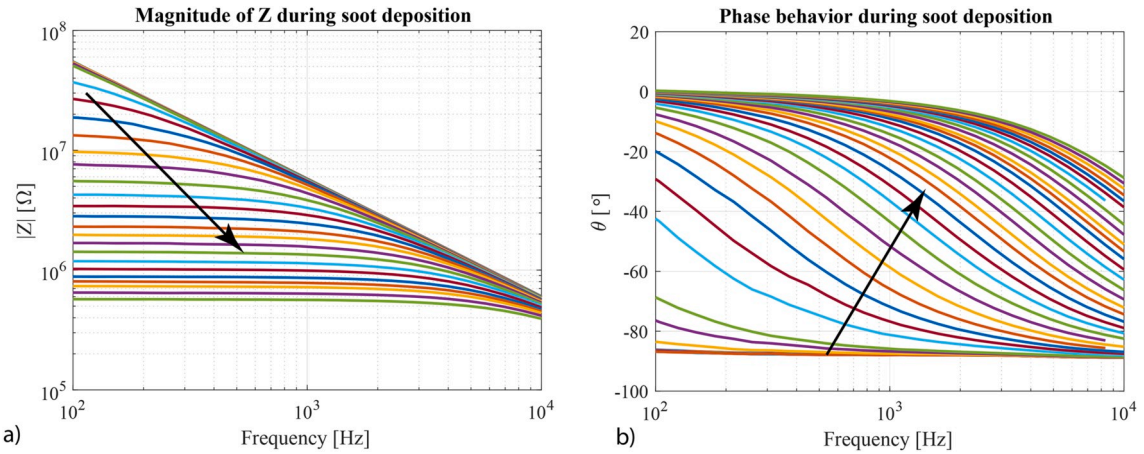

Fig. 6. a) The magnitude of the impedance Z for an in-plane IDE voltage of 3 V_{AC} and an voltage applied to the housing of 500 V_{DC}. The arrow indicates the direction of progressing time, while the time between each trace equals 1 min. b) The phase of the impedance $|Z|$, at an IDE voltage of 3 V_{AC} and a housing voltage of 500 V_{DC}. The arrow indicates the direction of progressing time, while the time between each trace equals 1 min. These plots show that the PM sensor behaves as a parallel resistor-capacitor circuit.

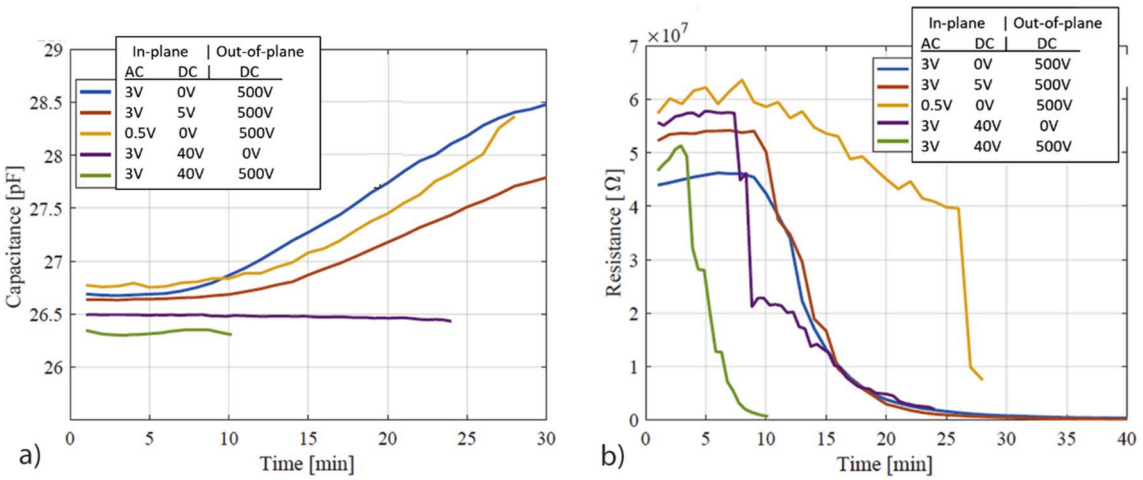

Fig. 7. (a) Extracted capacitance of the resistive PM sensor as a function of time and applied bias conditions. Samples with strong in-plane bias show suppressed capacitive response. Samples which develop capacitance increase over time exhibit typical resistive PM sensor response: delay followed by signal increase. b) Extracted resistance of the resistive PM sensor as a function of time. Soot bridges grow at a rate proportional to soot capture, directed by in-plane bias. Larger out-of-plane bias leads to much faster soot capture, and simultaneous large in-plane bias leads to inter-electrode directed dendrite growth. The resistance drops fastest for large out-of-plane and large in-plane bias. Resistance decreases slowest for the smallest in-plane bias.

consistent with the idea that both soot capture and dendrites follow electric field lines.

The impedance-derived capacitance traces also have strong variation with applied bias. However, it is notable that not all of the samples exhibit changed capacitive response as soot dendrites form. When large in-plane bias is applied, no change in capacitance is observed despite the evidence of dendrite formation in the dropping resistance. Similarly, when no out-of-plane bias is applied there is no change in capacitance. In samples where changed capacitance is observed, the time trace shows typical resistive PM sensor behavior that includes delay before capacitance rises. We also observe less rise in capacitance when increased DC bias is applied between the IDEs and when less AC bias is applied between the IDEs. We rationalize this behavior with our model: in order for capacitive response to occur in the resistive PM sensor, dendrites must move in response to the applied AC bias. This means that there will be an inherent delay while dendrites grow before a response can be observed. Additionally, the presence of dendrites does not guarantee that they have freedom of motion to participate in capacitive signal generation. When large in-plane DC bias is applied, the dendrites are constrained by electrical forces and cannot move in response to small in-plane AC bias, so no capacitance change can be measured. Similarly, when the inter-electrode bias is small, dendrites do not stand out of the IDE plane unless an out-of-plane bias is applied; when dendrites primarily lay in contact with the substrate plane they are not free to move in response to small AC bias, so no capacitive change is observed. Under conditions where dendrites are free to move, increasing in-plane DC bias reduces the dendrite freedom of motion in response to small AC bias, resulting in reduced change in capacitance. Further, reduced in-plane AC-bias provides a smaller electrical force to displace the dendrites and generate dipoles, so the capacitive response is smaller.

6. Discussion

Impedance spectroscopy has been applied to an IDE structure on a ceramic substrate, with the housing acting as an out-of-plane additional electrode to enable the application of a vertical E-field. Several combinations of horizontal and vertical E-fields are applied by electrically biasing the IDE and out-of-plane electrode, and the influence on deposited soot dendrites is studied.

Our experimental results are consistent with our model of the capacitive response of the resistive PM sensor. Microscopy reveals that soot dendrites grow out of the substrate plane, even when no out-of-plane bias is applied. Dendrites grow along electric field lines and the normal field component of in-plane bias is not negligible. This also means that increased in-plane bias does not lead to dendrites being pulled into the substrate plane; the most consistent way to get dendrites to solely reside in the substrate plane is to remove electric bias. The out-of-plane dendrites are influenced by the relative strength of electric and flow forces around them, so out-of-plane electric field can be used to hold the dendrites standing, and variation of lower magnitude forces like flow or in-plane electric field can be used to move dendrites around. According to our model, this manifests directly as the capacitive response of the device. An alternative explanation for the capacitive response, that inter-electrode area increases with dendrite growth, is not consistent with experimental observation for two reasons. First, we observe a delay before PM sensor capacitance increases, but soot dendrites are growing consistently for the entire time. If capacitance derives from dendrite surface area, we do not expect to see a delay before capacitance begins changing. Since our model relies on physical bending displacement of dendrites, it is consistent with a delay while dendrites grow to lengths where the balance of forces causes bending. Second, we observe no capacitive response when large in-plane bias is applied, despite the presence of inter-electrode dendrite bridges that cause reduced resistance. If capacitance is primarily caused by inter-electrode dendrite surface area, we would expect to see capacitive change in all of the applied bias conditions that we explored

in our impedance study. Our model is consistent with no capacitive response if the dendrites are constrained from bending by electric forces. A plausible explanation for disagreement with a capacitance increase caused by dendrite surface area is that the surface area change is negligible.

A more complete model of the resistive soot sensor therefore requires a description of dendrite growth and destruction, as in Bilby et al. (2016) and Grondin et al. (2019), as well as a description of how dendrites move in the force fields within the sensor, as we have begun to describe in this work. Our description focuses upon a change in relative dielectric constant and its impact on sensor capacitance, but dendrite motion also has the possibility to affect other aspects of device behavior, such as affecting the rate of soot capture due to dendrite orientation as is postulated in (Hopka, Bilby, & Van Nieuwstadt, 2017). It is possible that alternative operation modes could be developed based on designed motion of dendrites, for instance collapse of out-of-plane growth could be utilized to increase the total number of useable dendrite bridges. Further model development is needed to describe other aspects of dendrite motion.

This work could also lead to improvements in OBD applications of the PM sensor. For instance, if the relationship between PM sensor resistance and capacitance depends only upon soot dendrite properties, then a correlation could be used to perform an in-situ characterization of sensor gain stability. Similarly, our contribution to understanding the origin of the capacitive response of the sensor highlights different control sensitivities for this operation mode. This means that different optimization avenues, for instance designing relative in-plane and out-of-plane AC and DC electric fields, may be used for device optimization. Perhaps this will enable a faster responding device that does not suffer the limitations of the resistive measurement mode.

Finally, our contribution to understanding the origin of the capacitive response indicates that this mode does not require direct contact of the dendrites with both legs of the IDE. This means that non-conductive contamination on the IDE surface is not expected to degrade device performance, leading to the possibility of a more robust OBD device.

7. Conclusions

Impedance measurements from 100 Hz to 10 kHz supported the derived dendrite-IDE model, and it was found that the raw impedance data supports the equivalent circuit model of a parallel capacitor and resistor. Measurements also indicate that the capacitance increases more gradual with soot buildup as compared to the sudden reduction of resistance with dendrite formation. It remains to be investigated whether these time dependencies are sufficiently significant and repeatable. Morever, the exponential change in resistance, along with stochastic noise in dendrite growth, is generally undesired for accurate characterization of a DPF leak level, as the sensor is then treated as a switch rather than delivering a quantitative sensor signal.

We have also studied the influence of AC electric fields on the capacitive response of a resistive PM sensor. Our simulations of soot capture reinforce the understanding that PM is captured along electric field lines within the sensor, and that soot self-assembles into dendrites.

We propose a model for the origin of the capacitive response of the PM sensor that relies on bending motion of dendrites that stick up into space over the IDE. Our microscopy reveals that dendrites growing out of the plane of the substrate are sensitive to the electric and flow forces that are applied to them. We see dendrites moving as the relative strength of the forces change, confirming that the foundation of our model is tenable. Finally, our impedance analysis of the resistive PM sensor under different electric field application reveals capacitance that changes as our model predicts. The operation of the resistive PM sensor therefore relies not only on the electrical and self-assembly behavior of dendrites, but also on their freedom of motion. Future work includes further investigation of Micro-Electro Mechanical System (MEMS) technology for the fabrication of more repeatable cells, where the opposing electrodes both consists of an IDE.

Acknowledgement

The authors would like to thank M.M. Maricq for his valuable input during the review process.

References

Bartscherer, P., & Moos, R. (2013). Improvement of the sensitivity of a conductometric soot sensor by adding a conductive cover layer. *Journal of Sensors and Sensor Systems, 2*, 95–102.

Bilby, D., Kubinski, D. J., & Maricq, M. M. (2016). Current amplification in an electrostatic trap by soot dendrite growth and fragmentation: Application to soot sensors. *Journal of Aerosol Science, 98*, 41–58. https://doi.org/10.1016/j.jaerosci.2016.03.003. http://www.sciencedirect.com/science/article/pii/S002185021530104X.

Binnig, S., Fuchs, S., Collantes, C. R., & Volpp, H.-R. (2017). Exhaust gas condensate–formation, characterization and influence on platinum measuring electrodes in diesel vehicles. *Sensors and Actuators B: Chemical, 242*, 1251–1258.

Feulner, M., Hagen, G., Müller, A., Schott, A., Zöllner, C., Brüggemann, D., et al. (2015). Conductometric sensor for soot mass flow detection in exhausts of internal combustion engines. *Sensors, 15*(11), 28796–28806.

Fragkiadoulakis, P., Geivanidis, S., & Samaras, Z. (2018). Modeling a resistive soot sensor by particle deposition mechanisms. *Journal of Aerosol Science, 123*, 76–90.

Grob, B., Schmid, J., Ivleva, N. P., & Niessner, R. (2012). Conductivity for soot sensing: Possibilities and limitations. *Analytical Chemistry, 84*(8), 3586–3592.

Grondin, D., Breuil, P., Viricelle, J. P., & Vernoux, P. (2019). Modeling of the signal of a resistive soot sensor, influence of the soot nature and of the polarization voltage. *Sensors and Actuators B: Chemical, 298*, 126820. https://doi.org/10.1016/j.snb.2019.126820. http://www.sciencedirect.com/science/article/pii/S0925400519310196.

Grondin, D., Westermann, A., Breuil, P., Viricelle, J. P., & Vernoux, P. (2016). Influence of key parameters on the response of a resistive soot sensor. *Sensors and Actuators B: Chemical, 236*, 1036–1043. https://doi.org/10.1016/j.snb.2016.05.049. http://www.sciencedirect.com/science/article/pii/S0925400516307250.

Hagen, G., Riess, G., Schubert, M., Feulner, M., Müller, A., Brüggemann, D., et al. (2015). Capacitive soot sensor. *Procedia Engineering, 120*, 241–244.

Hagen, G., Spannbauer, C., Feulner, M., Kita, J., Müller, A., & Moos, R. (2018). Conductometric soot sensors: Internally caused thermophoresis as an important undesired side effect. *Sensors, 18*(10), 3531.

Harris, S. J., & Maricq, M. M. (2001). Signature size distributions for diesel and gasoline engine exhaust particulate matter. *Journal of Aerosol Science, 32*(6), 749–764.

Hopka, M. B., Bilby, D., & Van Nieuwstadt, M. (2017). Evaluation of non-contiguous pm measurements with a resistive particulate matter sensor. *SAE International Journal of Engines, 10*(4), 1683–1690.

Maricq, M. M. (2008). Thermal equilibration of soot charge distributions by coagulation. *Journal of Aerosol Science, 39*(2), 141–149.

Maricq, M. M., & Bilby, D. (2018). The impact of voltage and flow on the electrostatic soot sensor and the implications for its use as a diesel particulate filter monitor. *Journal of Aerosol Science, 124*, 41–53. https://doi.org/10.1016/j.jaerosci.2018.07.002. http://www.sciencedirect.com/science/article/pii/S002185021830154X.

Newell, K., Kartsonaki, C., Lam, K. B. H., & Kurmi, O. P. (2017). Cardiorespiratory health effects of particulate ambient air pollution exposure in low-income and middle-income countries: A systematic review and meta-analysis. *The Lancet Planetary Health, 1*(9). e368–e380.

Riehle, C., & Wadenpohl, C. (1996). Electrically stimulated agglomeration at an earthed surface. *Powder Technology, 86*(1), 119–126. https://doi.org/10.1016/0032-5910(95)03045-X. http://www.sciencedirect.com/science/article/pii/003259109503045X.

Rostedt, A., Ntziachristos, L. D., Simonen, P., Rönkkö, T., Samaras, Z. C., Hillamo, R., et al. (2017). A new miniaturized sensor for ultra-fast on-board soot concentration measurements. *SAE International Journal of Engines, 10*(4), 1859–1865.

Teike, G., Dietzel, M., Michaelis, B., Schomburg, H., & Sommerfeld, M. (2012). Multiscale lattice?Boltzmann approach for electrophoretic particle deposition. *Aerosol Science and Technology, 46*(4), 451–464.

Warey, A., Hendrix, B., Hall, M., & Nevius, T. (2004). A new sensor for on-board detection of particulate carbon mass emissions from engines. *SAE Transactions*, 1598–1605.

Zhang, Z., del Re, L., & Fuerhapter, R. (2017). Fast hybrid sensor for soot of production CI engines. In *Tech. rep., SAE Technical Paper*.